Nanoscale Energy Transport Dynamics across Nonbonded Solid–Molecule Interfaces and in Molecular Thin Films

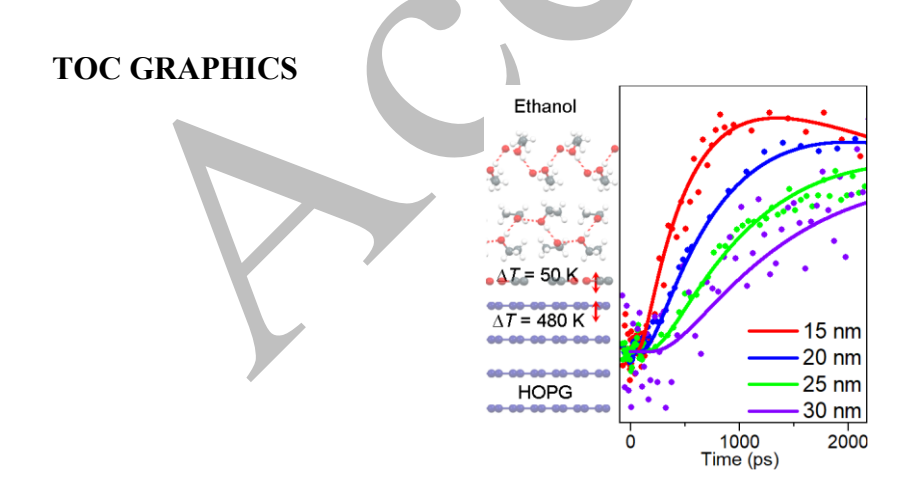
Xing He, Ding-Shyue Yang*

Department of Chemistry, University of Houston, Houston, TX 77204, United States

^{*}To whom correspondence should be addressed. Email: yang@uh.edu

ABSTRACT

Thermal conductance across a solid–solid interface requires an atomic/molecular-level understanding especially when a system is in a nonequilibrium state and/or consists of nanosized materials with prominent differences in structures, properties, and vibrational behaviors. Here, we report the lattice dynamics of graphite-supported molecular thin films of ethanol, whose layers exhibit in-plane hydrogen-bonded chains and out-of-plane van der Waals stacking with clear structural anisotropy. The direct structure-probing method of ultrafast electron diffraction reveals a surprising temperature difference of more than 400 K at picosecond to subnanosecond times across the graphite–ethanol interface, yet the temporal behavior signifies a reasonably large thermal boundary conductance. This apparent conflict in a nonequilibrium condition can be resolved by considering the coupling of out-of-plane motions, instead of the commonly-used temperature-based model, at transient times for energy transport across the interface separated by van der Waals interactions with mismatched unit sizes and no strong bonds. The importance of spatiotemporally-resolved structural dynamics at the atomic/molecular level is emphasized.



KEYWORDS van der Waals layers, interfacial motions, nonequilibrium heat transfer, thermal boundary resistance, Kapitza conductance

Heat transfer between two or more bodies in contact is ubiquitous and of practical significance. After two centuries of studies, the subject still attracts research attention on the fundamental principles involved. Today, complex architectures of modern electronic devices have reached the nanoscale. The incorporations of low-dimensional or functional materials are actively explored for new technological opportunities. The involvement of multiple nanoscale components in contact requires a thorough understanding of the cross-interface transport of energy carriers such as phonons, charges, plasmons, and their coupled phenomena. 1-3 A large body of the literature has been focused on solid-solid interfaces, where the composing particles (atoms or ions) often have similar sizes and are arranged in comparable lattice distances. The typical physical pictures used to explain interfacial thermal transport involve phonon scattering processes; the acoustic mismatch and diffuse mismatch models (AMM and DMM) are two continuum models that provide the theoretical limits of thermal boundary conductance, under the assumption of a thermalized phonon system on each side of an interface.^{4,5} However, it has been recognized that details of an interface at the nanoscale, which are ignored by AMM and DMM, may have prominent impacts on thermal resistance. 1, 2, 5, 6 Hence, recent theoretical investigations have often taken into account the atomistic nature of the interface in the calculations. 1, 2, 6 For example, the inclusion of a quantum-mechanical treatment on anharmonic scatterings has been considered for weakly-interacting van der Waals (vdW) interfaces.⁷

Experimentally, pump-probe thermoreflectance spectroscopy, especially the time-domain version of the technique, has been a major method to characterize interfacial thermal resistance.^{1, 5, 8} By fitting the data to a heat transport model with adjustable parameters, thermal properties such as the conductivity of thin films and the conductance of interfaces may be derived. However, additional information about transient structural changes at the atomic scale is not

obtained. In contrast, time-resolved diffraction-based methods have the advantage of direct structure-probing and the suitable spatiotemporal resolution for laser-induced lattice and phonon dynamics, in addition to thermal transport information. To date, studies concerning out-of-plane photothermally-induced dynamics have been conducted on substrate-supported elemental (semi)metal thin films, ⁹⁻¹⁶ semiconductor heterostructures, ¹⁷⁻¹⁹ two-dimensional materials, ^{20, 21} and water and methanol ices²²⁻²⁵ as well as a graphene-polymer interface. ²⁶ However, few reports looked into the energy transport across thin-film interfaces when two materials' composing units have significant size differences and are separated by weak (vdW) interactions. Such knowledge may be crucial to the developments of molecular-based optoelectronic devices.

In this report, the structural dynamics in graphite-supported ethanol thin films are examined by ultrafast electron diffraction (UED). The results are compared with those obtained in supported solid methanol, ²⁵ given that both molecules are capable of forming vdW-layered structures. Dynamically, the thermal transport from laser-heated graphite to nonbonded ethanol is found to be due to the coupling of atomic and molecular displacements at the interface; with decent thermal boundary conductance, it is surprising to see a temperature difference over hundreds of Kelvin at the graphite–ethanol interface. Further transport across the large vdW distances in a 2D-ordered ethanol thin film is incoherent and essentially diffusive in nature. However, for thinnest films studied, the coherent motions of the substrate surface and the lattice match at the interface cause additional modifications to the dynamic thermal-transport behavior at the nanoscale.

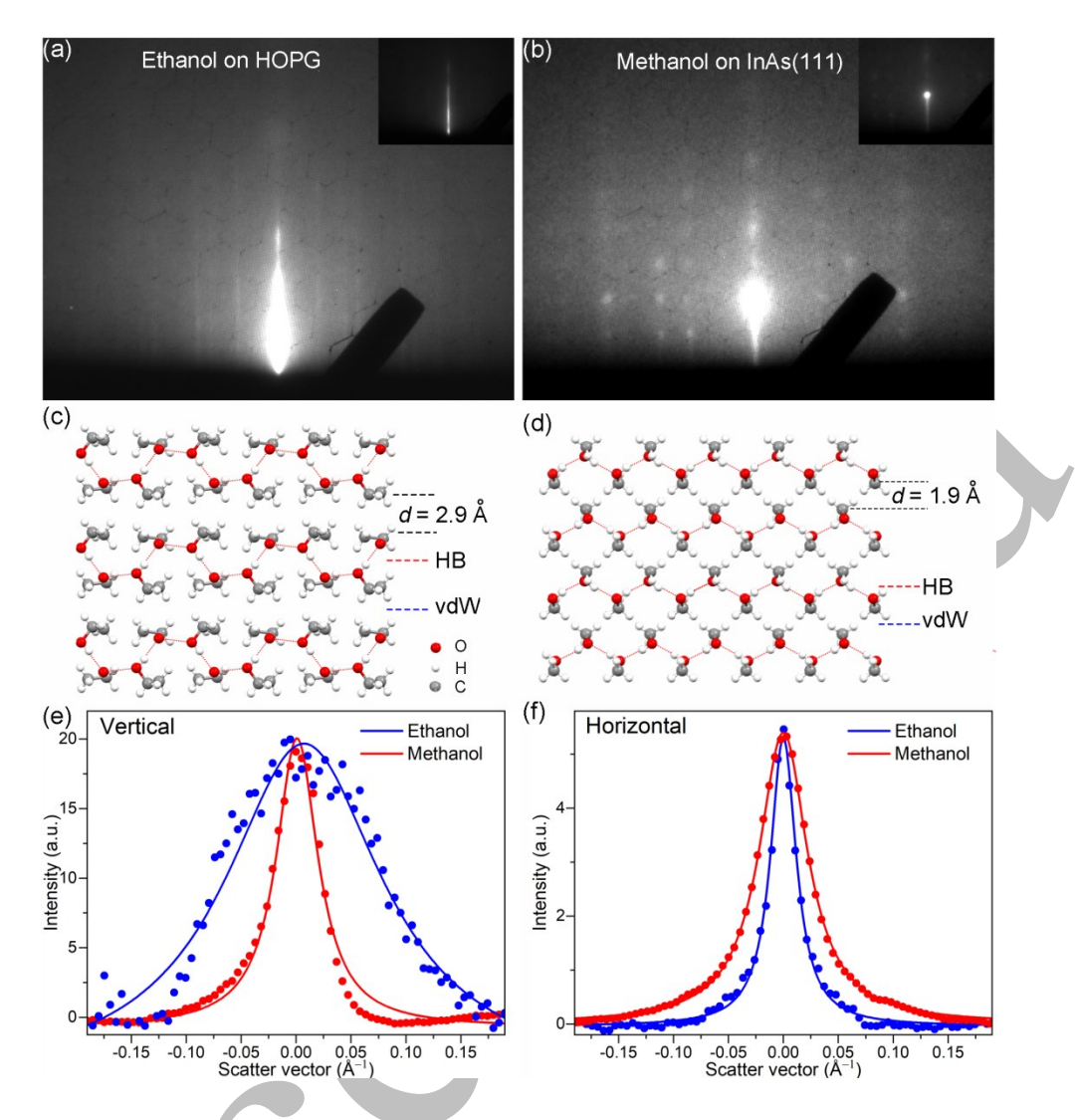


Figure 1. Diffractions and structures of annealed vapor-deposited solid ethanol and methanol. (a and b) Intensity-enhanced RHEED images acquired from films with a nominal thickness of 3 nm. The insets display the same images on a linear intensity scale. (c and d) Side view of monoclinic ethanol and orthorhombic methanol crystal structures (O, H, and C are in red, white, and gray, respectively). The alternating HB and vdW layers and the distance *d* between adjacent HB sheets are indicated. (e and f) Comparison of the vertical and horizontal intensity profiles of the diffractions from solid ethanol and methanol. The solid lines are fits of a Lorentzian function.

Shown in Figure 1a–d are the reflection high-energy electron diffraction (RHEED) images of annealed 3-nm-thick vapor-deposited ethanol (on highly-oriented pyrolytic graphite, HOPG) and methanol (on smooth InAs(111)) as well as their respective crystal structures. The

temperature- and thickness-dependent structural evolutions of ethanol and methanol thin films have been reported previously.^{27, 28} Here, the attention is on the structural differences and crystallinity of the films. The two molecular solids share many similarities, including the mass density, hydrogen-bonded (HB) chains that are infinitely extended along only one crystal axis, aliphatic vdW forces between adjacent chains to form a 2D molecular sheet, and vdW interactions between stacked layers along the out-of-plane direction. The major structural differences are that (i) the ethanol HB chains are puckered whereas the methanol ones are zigzagged, and (ii) the vdW-layer (adjacent C-C vertical) distances are about 2.9 and 1.9 Å for ethanol and methanol, respectively. Hence, solid ethanol exhibits a weaker interlayer interaction per molecule and a denser HB single sheet. Experimentally, unlike methanol, ethanol thin films do not produce sharp Bragg spots along the vertical direction upon thermal annealing, which signifies a poor stacking and the difficulty in the 2D-to-3D transformation for the growth of the cross-plane order (Figure 1e).^{27, 28} The horizontal domain sizes are more comparable according to the Scherrer formula calculation based on the horizontal diffraction widths,²⁹ where solid ethanol shows about 3.6 times larger domain size than methanol, which is consistent with the former having a denser HB network (Figure 1f). Thus, 2D-ordered, vdW-stacked ethanol thin films annealed up to ~120 K are used in the current dynamics study (following the consideration to minimize sublimation loss during the thermal treatment in vacuum and the possible impact of the interfacial structure²⁸).

The method of UED is used to examine how atomic and molecular motions are coupled in the HOPG-ethanol system, where the probed depth in the top of an ethanol film is estimated to be ~2.0 nm according to the elastic mean free path of 30-keV electrons and an incidence angle of around 1.0° (See Supplementary Information for the Experimental Section). Previous reports

have established the photodynamics of bare graphite on the sub-ps to sub-ns temporal scale. 30-34 Initially, photoexcitation injects energy into the electron system, and the majority of it transfers to strongly-coupled optical phonons in ~500 fs followed by their decays into other select phonons. Coherent lattice motions in the in-plane and out-of-plane directions also play a role in addition to the phonon-initiated atomic motions. A slower time constant of ~7 ps was found for further electron-phonon coupling and phonon equilibration. On such a time scale, graphite's lattice is heated and its structural dynamics along all directions are essentially thermal in nature, followed by slow heat dissipation into the bulk over longer times. Thus, for the purpose of this study, the photoinduced dynamics of the HOPG substrate may be regarded as an impulsive source of thermal atomic motions underneath the supported ethanol molecules with a rise time constant of ~7 ps and slow dissipation. At the laser fluence of 6.6 mJ/cm² at 1030 nm, a surface temperature jump of $\Delta T_{\rm G_{max}} \simeq 480~{\rm K}$ is estimated from a base temperature of 100 K, using a temperature-dependent specific heat of graphite.^{35, 36} Now the questions are (i) how the vdWstacked ethanol layers respond to the impulsively heated substrate surface and (ii) how the interfacial structure may influence the coupling of motions.

Shown in Figure 2 are the RHEED and UED images of a 25-nm ethanol thin film, annealed up to 120 K and then maintained at 100 K. The increase in the horizontal diffraction width in panels b and c results from the use of a moderately converging beam (to minimize the electron footprint on the sample), which leads to its diverging downstream on the imaging device. The clear center diffraction streak without a narrow vertical width signifies the 2D-layered nature of the ethanol assembly lacking a well-defined stacking order between layers. Following the heating impulse of the supporting HOPG, a decrease in the intensity is observed along the streak, which signifies an increase in out-of-plane molecular motions that perturb the

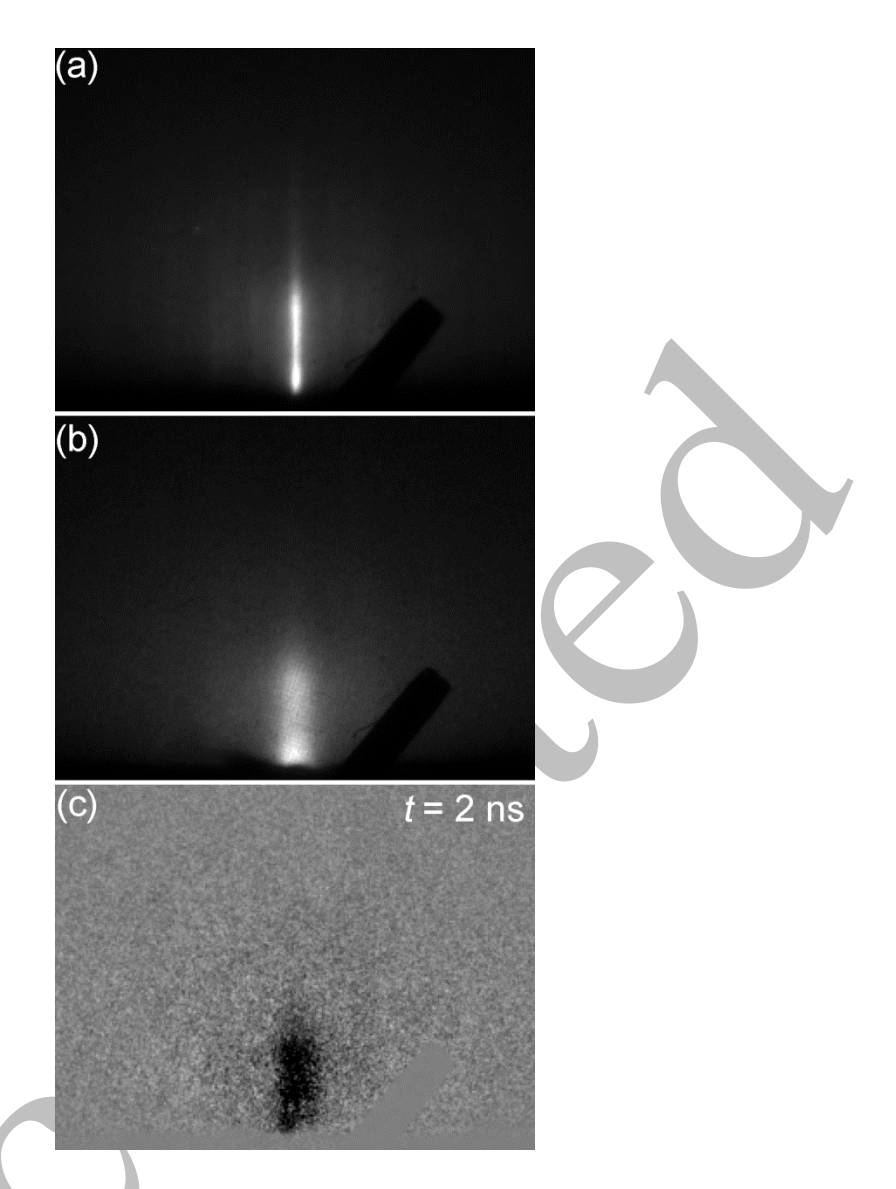


Figure 2. RHEED and UED images of 2D-layered ethanol films. (a) Diffraction from 25-nm solid ethanol obtained with a collimated electron beam. (b) Diffraction from the same film acquired with a moderately focused beam. (c) Difference image at 2 ns referenced with a negative-time frame, which shows the decrease from the initial intensity in black. The grey color refers to no or negligible intensity changes.

equilibrium lattice order observed in the top nanometers of a thin film. The specific sensitivity along the vertical vdW direction is given by the reflection probing geometry according to the Debye–Waller mechanism,

$$\ln(I_0/I(t)) = 2W(t) = \Delta \langle (\vec{q} \cdot \vec{u}(t))^2 \rangle = 4\pi^2 s_\perp^2 \cdot \Delta \langle u_\perp^2(t) \rangle \tag{1}$$

where the I_0 and I(t) are the diffraction intensities before the zero of time and at time t after the heating impulse, respectively, W the Debye–Waller factor, \vec{u} the molecular displacement vector, $\vec{q} = 2\pi \vec{s}_{\perp}$ the scattering vector, and $s_{\perp} = 2\sin(\theta/2)/\lambda$ the vertical momentum transfer along the surface normal direction, with θ being the total scattering angle and $\lambda = 0.0698$ Å the de Broglie wavelength of 30-keV electrons. $\Delta \langle u_{\perp}^2(t) \rangle$ is the change in the out-of-plane component of the mean-square displacements (MSD). We rule out the possibility of photogenerated surface transient electric fields as the cause for the observed diffraction change, as we note the absence of notable intensity modulations near the shadow edge at the laser fluences used (Figure 2c). ^{21, 25, 37} Also, the reproducible images and dynamics recorded over many time scans indicate no noticeable loss of the thin films due to repeated laser heating at 1 kHz of the fluence used.

It is found that an intensity decrease of $\sim 8\%$ is eventually reached at a time dependent on the film thickness, which signifies the gain of $\Delta \langle u_{\perp}^2 \rangle$ to be ~ 0.013 Å². This means a temperature increase of $\Delta T \simeq 50$ K near the top of the films according to the Debye model,

$$\langle u_{\perp}^{2}(T)\rangle = \frac{3\hbar^{2}}{mk_{\rm B}\Theta_{\rm D}} \left[\frac{1}{4} + \left(\frac{T}{\Theta_{\rm D}} \right)^{2} \int_{0}^{\Theta_{\rm D}/T} \frac{x dx}{e^{x} - 1} \right] \cong \frac{3\hbar^{2}T}{mk_{\rm B}\Theta_{\rm D}^{2}}$$
(2)

where $\hbar = h/2\pi$ is the reduced Planck constant, m the mass of an ethanol molecule, $k_{\rm B}$ the Boltzmann constant, and $\Theta_{\rm D}$ is the Debye temperature, which is 112 K for crystalline ethanol.³⁸ Such an increase appears to be consistent with the following two findings. First, the temperature jump on the sub-ns to ns scale is below the thermodynamic melting point of 159 K and not too high above the steady-state evaporation temperature above 140 K, which agrees with the observation of a fully recoverable ground state. Second, a loss of the deposited ethanol film does occur at a higher fluence, which implies the existence of an upper limit for the tolerable transient ΔT that is not much higher than the observed value here.

However, there seems to be a glaring difference between the temperature jumps of the substrate surface and a molecular thin film: How could ethanol molecules remain assembled above a transiently highly heated surface? Theoretically, without any other channel for thermal flow, the temperature of a supported thin film should keep rising until it is close to that of the supporting surface, according to Fourier's law and the equation for the Kapitza conductance³⁹

$$C\rho d\frac{\partial T(t)}{\partial t} = -\sigma[T(t) - T_{G}(z_{G} = 0, t)]$$
(3)

where C = 1.38 J/(g·K) and $\rho = 1.025$ g/cm³ are the specific heat⁴⁰ and density of crystalline ethanol at 100 K, respectively, d the film thickness, σ the thermal boundary conductance, and $T_G(z,t)$ is the temperature of HOPG at depth z_G and time t. Given the slow decrease of T_G ,

$$\Delta T(t) \sim \Delta T_{\rm G}(0,t) - \Delta T_{\rm G_{\rm max}} \exp(-\sigma t/\mathcal{C}\rho d)$$
 (4)

which signifies the approach of $\Delta T(t)$ toward ΔT_G . We obtain $\sigma \simeq 57$ MW/(m²·K) from the approximate rise time of $C\rho d/\sigma \simeq 370$ ps from the data of d=15 nm. Such a σ value is within the reasonable range for vibrational heat conduction across interfaces between crystalline solids² and higher than those of some solid-state materials.^{21,41} Thus, the obvious inconsistence between $\Delta T(t)$ and ΔT_G indicates the inadequacy of the phenomenological model of thermal boundary conductance.

We argue that at the nanoscale, a molecular-level understanding is needed to visualize how the transfer of kinetic energy takes place across the interface, especially for two- or multi-layer systems with relatively weak interactions and appreciably different unit sizes (between overlaying molecules and atoms of a supporting solid). Here, it is important to note that the out-of-plane root-mean-square displacement (RMSD) of the HOPG surface is ~0.058 Å at 100 K and ~0.091 Å at 580 K, calculated using the middle expression of Equation 2 with the Debye temperature of 950 K⁴² and the mass of a carbon atom for *m*. The increase in the vertical RMSD

is therefore ~0.033 Å. In a thin film, the vertical RMSD of an ethanol molecule is about 0.158 Å at 100 K and 0.195 Å at the elevated temperature of ~150 K, which, coincidentally, exhibits about the same amount of increase. Such a match of increased RMSDs provides strong evidence for a movement-based picture for energy transport across a nonbonded interface to a soft material, instead of a simple temperature-based model (see below).

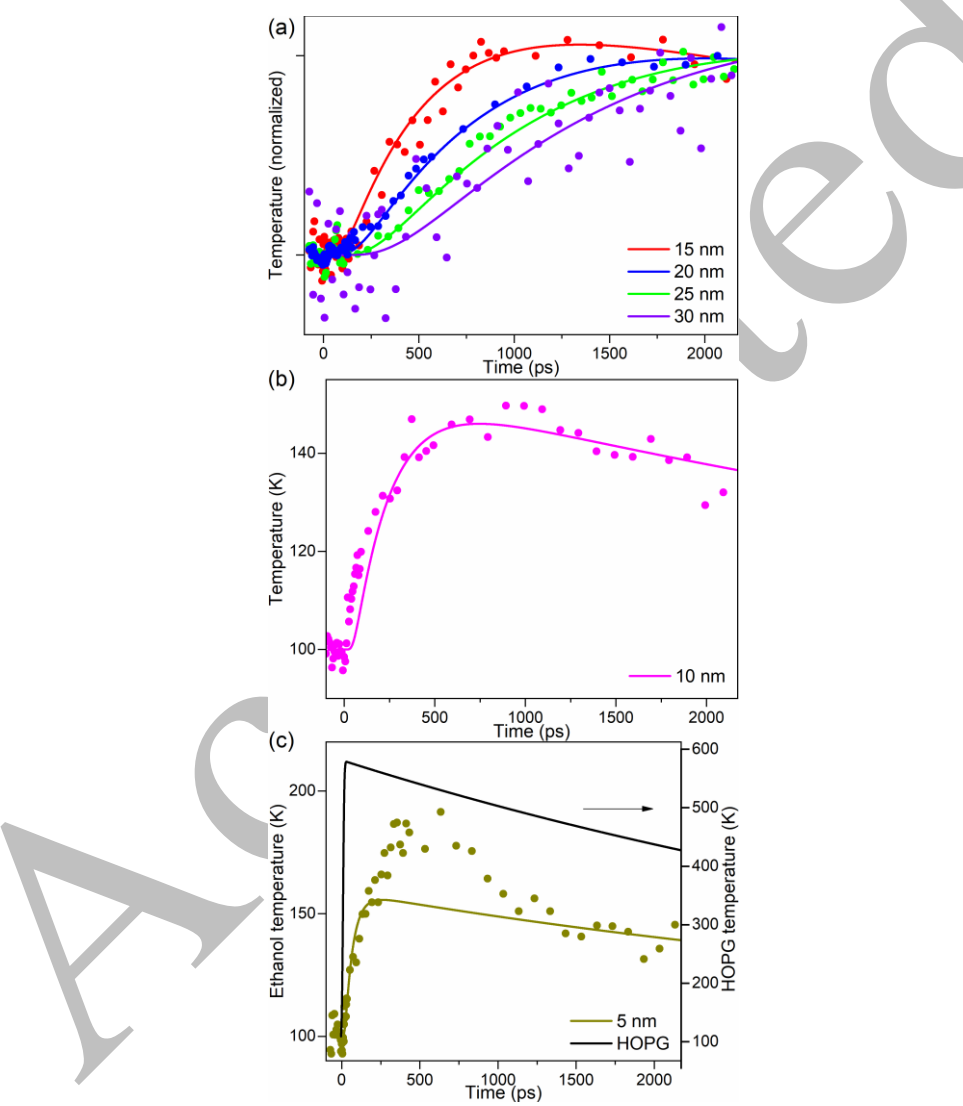


Figure 3. Time-dependent dynamics of 2D-layered ethanol thin films with a nominal thickness of (a) 15 to 30 nm, (b) 10 nm, and (c) 5 nm. The solid lines are the theoretical curves based on a thermal diffusion model. The agreement is satisfactory for thicker films, whereas larger deviation is seen for the thinnest film studied. The black solid line in (c) is the temperature of the HOPG substrate surface derived from a UED experiment.

Following the RMSD coupling at the interface, the increased molecular motions around the assembly's lattice positions ensue and propagate across a thin film. The motions' effect on the diffraction intensity is measured from the top nanometers and exhibits prominent thickness dependence. We find that the UED results of 15- to 30-nm films can be explained using the 1D thermal diffusion equation,

$$\frac{\partial T(z,t)}{\partial t} = \frac{K}{\rho C} \frac{\partial^2 T(z,t)}{\partial z^2} \tag{5}$$

where K = 0.28 W/(m·K) is the thermal conductivity of solid ethanol obtained, which agrees well with the literature value for an ordered crystal⁴³ and is comparable to the value of 0.36 W/(m·K) for crystalline methanol.^{25, 44} With the theoretical model also used in a previous report,²⁵ the agreement between the experimental observations and the simulation results is satisfactory (Figure 3a); the rise, decay, and onset delay of the dynamics are reproduced (see Supplementary Information for further details of the model). Hence, the thermal transport mechanism in sufficiently thick ethanol films is diffusive in nature. However, as the film thickness decreases, some deviations are noticed. For 10 nm, the diffusion model does not capture the faster rise seen in the first 250 ps, although the slow recovery part after 500 ps seems to match well (Figure 3b). The disagreement for the 5-nm case is even more prominent, where the experimental data suggest a higher temperature rise (or a larger-than-anticipated out-of-plane MSD before the conversion using Equations 1 and 2) in a few hundred ps followed by a decay seemingly faster than the rate of the supporting substrate (Figure 3c). If a temperature jump similar to those of thicker films is used, the simulation curve can be made to match with the early rise and later recovery, but disagreement is found for a duration of ~1 ns.

Taking all observed features of the structural dynamics together, we believe that the following RMSD-based picture provides an intuitive and adequate explanation. In the current

graphite-ethanol system, vast differences are seen in (i) the strengths of the chemical bonds in graphite, the interactions between the graphene lattice and the near-commensurate interfacial ethanol.²⁸ and the vdW forces between HB ethanol layers; and (ii) the sizes and masses of the atomic and molecular constituents across the interface, the lattice constants, and orders of the packing on two sides of the interface. It may not be straightforward to explain the interfacial thermal transport considering the distinctly different vibrational properties and spectra. However, from an atomic/molecular viewpoint, the RMSDs of graphite's carbon atoms acquire a fast jump following the pulsed laser excitation and phonon thermalization. For the *incoherent* motion part, the moderate amount of the RMSD increase is governed by graphite's larger Debye temperature although the temperature jump is high. On such a "quivering" surface, overlaying larger molecules (separated by the vdW distances of a few Å) experience the underlying incoherent motions and transferring of kinetic energy, and thus a similar amount of their vertical RMSD increase (merely one to few per cent of the spacing) is resulted in order to maintain the average interfacial distance. The good coupling of the RMSDs, experimentally supported by the decent σ value, is anticipated given the immediate contact (and presumably a reasonable overlap of the low-frequency part of the lattice vibrational spectra). However, the softness and low Debye temperature of the molecular film mean that the effective temperature jump is limited and far below that of the substrate. Hence, the phenomenon of volatile molecules holding onto a pulsedlaser-heated surface can be understood. Afterward, molecules in upper HB ethanol layers (separated in ~3 Å by vdW forces) also experience a higher RMSD from underneath and therefore incur a similar extent of increased motions around their equilibrium positions in the lattice. The UED results of thicker ethanol films indicate the incoherent nature of the process, which should have a strong connection with the structural noncrystallinity vertically. Hence, a

thermal diffusion model can capture the transport dynamics of the lattice motions well.

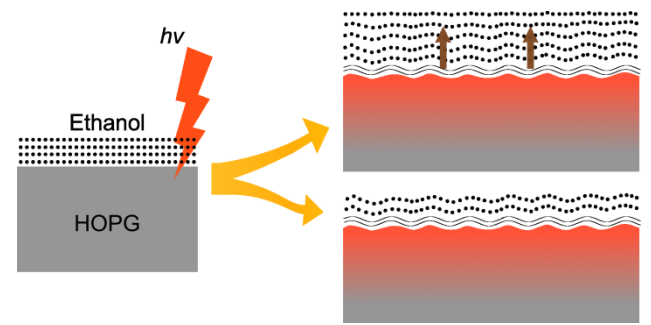


Figure 4. Schematic of the motion-coupled energy transport at the photoexcited graphite—ethanol interface. At early times, the coherent phonon motions of the top graphene layer are depicted by the wavy substrate surface (not drawn in scale). The incoherent thermal motions of carbon atoms are represented by the color gradient in the substrate block. (Lower) At a low thickness, the quivering graphite surface incites relatively fast and large displacements of ethanol molecules in the interfacial assembly structure and upper layers. (Upper) At a larger thickness, the vdW weak coupling between adjacent ethanol layers causes incoherence of displacement motions, leading to effectively diffusion-like thermal transport to the top on a longer time scale (brown arrows).

For low thicknesses, we need to consider the effects of the *coherent* part of the substrate atoms' motions and the near-commensurate lattice match at the interface (Figure 4). It is known that coherent acoustic phonons (CAPs) across the stacked layers of graphite are also dynamically induced following laser excitation, ^{33, 45} which cause additional amplitudes in the vertical motions at the solid-molecule interface that can push overlaying molecules further. Such CAP motions are wavelike and may therefore incite a much faster response in adjacent molecular layers compared to the diffusion-based prediction (early-time dynamics in Figure 3b; schematic in Figure 4, lower). Furthermore, the combined effects from the substrate surface's coherent and incoherent motions (and possibly the good match of the in-plane structures²⁸ for a better dynamic coupling) may lead to a larger dynamic change as seen in Figure 3c for the thinnest film studied, where an accumulation of larger RMSDs is produced in the molecular film via driven oscillation motions in a weakly-coupled, vdW-layered lattice. However, at longer times as the substrate

continues to relax, a faster dissipation of the additional molecular RMSDs is seen until the rate matches the theoretical prediction. We further note that the enhanced interfacial coupling quickly diminishes as the film thickness increases, which is in line with the interfacial structure transitioning to the bulk-like layers after ~2 nm away from the graphite surface, as well as the structural inhomogeneity along the layer-stacking direction (Figure 4, upper).

Essentially, the same mechanism is found applicable to the thermal-transport dynamics for both the graphite–2D-ethanol and InAs–2D-methanol systems at the nanoscale, with RMSD-matched coupling at the interface and diffusive transport across molecules in vdW-spaced HB layers. The commonality signifies the key role of atomic/molecular displacements and incoherently-driven motions in the flow of thermal energy across nonbonded constituents and interfaces; given the direct contact, the different vdW distances (Figure 1, c and d) do not have a fundamental impact. However, differences still exist between the behaviors of assemblies of the two structurally similar molecules. First, it is difficult for ethanol thin films to form a good vertical stacking order and adopt more ballistic-type transport as methanol assemblies can via careful annealing. Second, it is intriguing to see a faster-than-theory rise of dynamic changes in a 10-nm ethanol film (Figure 3b), whereas a 2D-layered methanol film of the same nominal thickness exhibits the predicted dynamics. We hypothesize that the larger lateral HB network size for ethanol as well as the presence of a near-commensurate interfacial structure to mediate the coupling modify the collective motions of the molecules but in a limited nanoscale range.

In summary, UED is used as a time-resolved direct-structure-probing method to visualize the thermal-transport dynamics of graphite-supported HB ethanol films. For such a nonbonded two-component system with largely different vibrational properties and interlayer vdW spaces, it is found that the phenomenological conductance model is not adequate to account for the vast

difference in materials' temperatures across the interface at transient times. Instead, a

microscopic model considering the same amount of increase in the atomic and molecular

displacements provides the explanation for the interfacial coupling of transient motions. The

significance of such dynamics is consistent with the findings of interfacial phonon modes at the

interface within a limited range of ~1 nm⁴⁶ and the dominant contribution of out-of-plane

vibrations to energy transfer at weakly-interacting interfaces. 47 Although the thermal transport in

a poorly-stacked thicker molecular assembly is diffusive in nature and slow, faster changes can

be observed at the nanoscale when collective molecular motions are facilitated by the lateral

crystalline order, to compensate for (or even outweigh) the incoherent behavior originating from

the inhomogeneity of the out-of-plane stacking. Our structural dynamics obtained with a sub-

ps/ps impulse reveal the structure—behavior relation. It will be interesting to compare with results

acquired from other interfacial systems with different bonding, packing orders, and vibrational

spectral overlaps.

ASSOCIATED CONTENT

Supporting Information

Experimental section, simulation of thermal diffusion in a supported ethanol assembly

AUTHOR INFORMATION

Corresponding Author

*Email: yang@uh.edu Phone: +1 713-743-6022.

ORCID

Xing He: 0000-0001-5341-5662

Ding-Shyue Yang: 0000-0003-2713-9128

16

Notes

The authors declare no competing financial interests.

ACKNOWLEDGMENT

This research was supported by the National Science Foundation (CHE-2154363 and CHE-1653903). Partial support from the R. A. Welch Foundation (E-1860) for instrumental developments is acknowledged.

REFERENCES

- 1. Chen, J.; Xu, X. F.; Zhou, J.; Li, B. W. Interfacial Thermal Resistance: Past, Present, and Future. *Rev. Mod. Phys.* **2022**, *94*, 025002.
- 2. Giri, A.; Hopkins, P. E. A Review of Experimental and Computational Advances in Thermal Boundary Conductance and Nanoscale Thermal Transport across Solid Interfaces. *Adv. Funct. Mater.* **2020**, *30*, 1903857.
- 3. Giri, A.; Walton, S. G.; Tomko, J.; Bhatt, N.; Johnson, M. J.; Boris, D. R.; Lu, G. Y.; Caldwell, J. D.; Prezhdo, O. V.; Hopkins, P. E. Ultrafast and Nanoscale Energy Transduction Mechanisms and Coupled Thermal Transport across Interfaces. *ACS Nano* **2023**, 10.1021/acsnano.3c02417.
- 4. Swartz, E. T.; Pohl, R. O. Thermal Boundary Resistance. Rev. Mod. Phys. 1989, 61, 605-668.
- 5. Cahill, D. G.; Ford, W. K.; Goodson, K. E.; Mahan, G. D.; Majumdar, A.; Maris, H. J.; Merlin, R.; Phillpot, S. R. Nanoscale Thermal Transport. *J. Appl. Phys.* **2003**, *93*, 793-818.
- 6. Hopkins, P. E. Thermal Transport across Solid Interfaces with Nanoscale Imperfections: Effects of Roughness, Disorder, Dislocations, and Bonding on Thermal Boundary Conductance. *ISRN Mech. Eng.* **2013**, *2013*, 682586.
- 7. Zhou, H. B.; Zhang, G.; Wang, J.-S.; Zhang, Y.-W. Anharmonic Quantum Thermal Transport across a van der Waals Interface. *MRS Bull.* **2023**, *48*, 614-622.

- 8. Cahill, D. G.; Braun, P. V.; Chen, G.; Clarke, D. R.; Fan, S. H.; Goodson, K. E.; Keblinski, P.; King, W. P.; Mahan, G. D.; Majumdar, A.; Maris, H. J.; Phillpot, S. R.; Pop, E.; Shi, L. Nanoscale Thermal Transport. II. 2003-2012. *Appl. Phys. Rev.* **2014**, *1*, 011305.
- 9. Highland, M.; Gundrum, B. C.; Koh, Y. K.; Averback, R. S.; Cahill, D. G.; Elarde, V. C.; Coleman, J. J.; Walko, D. A.; Landahl, E. C. Ballistic-Phonon Heat Conduction at the Nanoscale as Revealed by Time-Resolved X-Ray Diffraction and Time-Domain Thermoreflectance. *Phys. Rev. B* **2007**, *76*, 075337.
- Siemens, M. E.; Li, Q.; Yang, R. G.; Nelson, K. A.; Anderson, E. H.; Murnane, M. M.;
 Kapteyn, H. C. Quasi-Ballistic Thermal Transport from Nanoscale Interfaces Observed
 Using Ultrafast Coherent Soft X-Ray Beams. *Nat. Mater.* 2010, 9, 26-30.
- 11. Sokolowski-Tinten, K.; Li, R. K.; Reid, A. H.; Weathersby, S. P.; Quirin, F.; Chase, T.; Coffee, R.; Corbett, J.; Fry, A.; Hartmann, N.; Hast, C.; Hettel, R.; Horn von Hoegen, M.; Janoschka, D.; Lewandowski, J. R.; Ligges, M.; Meyer zu Heringdorf, F.; Shen, X.; Vecchione, T.; Witt, C.; Wu, J.; Dürr, H. A.; Wang, X. J. Thickness-Dependent Electron-Lattice Equilibration in Laser-Excited Thin Bismuth Films. *New J. Phys.* **2015**, *17*, 113047.
- Sokolowski-Tinten, K.; Shen, X.; Zheng, Q.; Chase, T.; Coffee, R.; Jerman, M.; Li, R. K.; Ligges, M.; Makasyuk, I.; Mo, M.; Reid, A. H.; Rethfeld, B.; Vecchione, T.; Weathersby, S. P.; Dürr, H. A.; Wang, X. J. Electron-Lattice Energy Relaxation in Laser-Excited Thin-Film Au-Insulator Heterostructures Studied by Ultrafast MeV Electron Diffraction. *Struct. Dyn.* 2017, 4, 054501.
- 13. Pudell, J.; Maznev, A. A.; Herzog, M.; Kronseder, M.; Back, C. H.; Malinowski, G.; von Reppert, A.; Bargheer, M. Layer Specific Observation of Slow Thermal Equilibration in Ultrathin Metallic Nanostructures by Femtosecond X-Ray Diffraction. *Nat. Commun.* **2018**, *9*, 3335.
- 14. Hanisch, A.; Krenzer, B.; Pelka, T.; Mollenbeck, S.; Horn-von Hoegen, M. Thermal Response of Epitaxial Thin Bi Films on Si(001) Upon Femtosecond Laser Excitation Studied by Ultrafast Electron Diffraction. *Phys. Rev. B* **2008**, *77*, 125410.
- 15. Hanisch-Blicharski, A.; Krenzer, B.; Wall, S.; Kalus, A.; Frigge, T.; Horn-von Hoegen, M. Heat Transport through Interfaces with and without Misfit Dislocation Arrays. *J. Mater. Res.* **2012**, *27*, 2718-2723.

- 16. Hanisch-Blicharski, A.; Tinnemann, V.; Wall, S.; Thiemann, F.; Groven, T.; Fortmann, J.; Tajik, M.; Brand, C.; Frost, B.-O.; von Hoegen, A.; Horn-von Hoegen, M. Violation of Boltzmann Equipartition Theorem in Angular Phonon Phase Space Slows Down Nanoscale Heat Transfer in Ultrathin Heterofilms. *Nano Lett.* 2021, 21, 7145-7151.
- Bargheer, M.; Zhavoronkov, N.; Gritsai, Y.; Woo, J. C.; Kim, D. S.; Woerner, M.; Elsaesser,
 T. Coherent Atomic Motions in a Nanostructure Studied by Femtosecond X-Ray Diffraction.
 Science 2004, 306, 1771-1773.
- Lee, S. H.; Cavalieri, A. L.; Fritz, D. M.; Swan, M. C.; Hegde, R. S.; Reason, M.; Goldman, R. S.; Reis, D. A. Generation and Propagation of a Picosecond Acoustic Pulse at a Buried Interface: Time-Resolved X-Ray Diffraction Measurements. *Phys. Rev. Lett.* 2005, 95, 246104.
- 19. Gorfien, M.; Wang, H. L.; Chen, L.; Rahmani, H.; Yu, J. X.; Zhu, P. F.; Chen, J.; Wang, X.; Zhao, J. H.; Cao, J. M. Nanoscale Thermal Transport across an GaAs/Algaas Heterostructure Interface. *Struct. Dyn.* **2020,** *7*, 025101.
- 20. Tung, I.-C.; Krishnamoorthy, A.; Sadasivam, S.; Zhou, H.; Zhang, Q.; Seyler, K. L.; Clark, G.; Mannebach, E. M.; Nyby, C.; Ernst, F.; Zhu, D. L.; Glownia, J. M.; Kozina, M. E.; Song, S.; Nelson, S.; Kumazoe, H.; Shimojo, F.; Kalia, R. K.; Vashishta, P.; Darancet, P.; Heinz, T. F.; Nakano, A.; Xu, X. D.; Lindenberg, A. M.; Wen, H. D. Anisotropic Structural Dynamics of Monolayer Crystals Revealed by Femtosecond Surface X-Ray Scattering. *Nat. Photonics* 2019, *13*, 425-430.
- 21. He, X.; Chebl, M.; Yang, D.-S. Cross-Examination of Ultrafast Structural, Interfacial, and Carrier Dynamics of Supported Monolayer MoS₂. *Nano Lett* **2020**, *20*, 2026-2033.
- 22. Ruan, C.-Y.; Lobastov, V. A.; Vigliotti, F.; Chen, S. Y.; Zewail, A. H. Ultrafast Electron Crystallography of Interfacial Water. *Science* **2004**, *304*, 80-84.
- 23. Yang, D.-S.; Zewail, A. H. Ordered Water Structure at Hydrophobic Graphite Interfaces Observed by 4D, Ultrafast Electron Crystallography. *Proc. Natl. Acad. Sci. USA* **2009**, *106*, 4122-4126.
- 24. Yang, D.-S.; He, X. Structures and Ultrafast Dynamics of Interfacial Water Assemblies on Smooth Hydrophobic Surfaces. *Chem. Phys. Lett.* **2017**, *683*, 625-632.
- 25. He, X.; Yang, D.-S. Order-Determined Structural and Energy Transport Dynamics in Solid-Supported Interfacial Methanol. *Nano Lett.* **2021**, *21*, 1440-1445.

- 26. Gulde, M.; Schweda, S.; Storeck, G.; Maiti, M.; Yu, H. K.; Wodtke, A. M.; Schäfer, S.; Ropers, C. Ultrafast Low-Energy Electron Diffraction in Transmission Resolves Polymer/Graphene Superstructure Dynamics. *Science* 2014, 345, 200-204.
- 27. He, X.; Wu, C. Y.; Yang, D.-S. Communication: No Guidance Needed: Ordered Structures and Transformations of Thin Methanol Ice on Hydrophobic Surfaces. *J. Chem. Phys.* **2016**, *145*, 171102.
- 28. He, X.; Yang, D.-S. Ethanol on Graphite: Ordered Structures and Delicate Balance of Interfacial and Intermolecular Forces. *J. Phys. Chem. C* **2021**, *125*, 24145-24154.
- 29. Patterson, A. L. The Scherrer Formula for X-Ray Particle Size Determination. *Phys. Rev.* **1939,** *56*, 978-982.
- 30. Carbone, F.; Baum, P.; Rudolf, P.; Zewail, A. H. Structural Preablation Dynamics of Graphite Observed by Ultrafast Electron Crystallography. *Phys. Rev. Lett.* **2008**, *100*, 035501.
- 31. Raman, R. K.; Murooka, Y.; Ruan, C.-Y.; Yang, T.; Berber, S.; Tománek, D. Direct Observation of Optically Induced Transient Structures in Graphite Using Ultrafast Electron Crystallography. *Phys. Rev. Lett.* **2008**, *101*, 077401.
- 32. Harb, M.; Jurgilaitis, A.; Enquist, H.; Nüske, R.; Schmising, C. v. K.; Gaudin, J.; Johnson, S. L.; Milne, C. J.; Beaud, P.; Vorobeva, E.; Caviezel, A.; Mariager, S. O.; Ingold, G.; Larsson, J. Picosecond Dynamics of Laser-Induced Strain in Graphite. *Phys. Rev. B* **2011**, *84*, 045435.
- 33. Chatelain, R. P.; Morrison, V. R.; Klarenaar, B. L. M.; Siwick, B. J. Coherent and Incoherent Electron-Phonon Coupling in Graphite Observed with Radio-Frequency Compressed Ultrafast Electron Diffraction. *Phys. Rev. Lett.* **2014**, *113*, 235502.
- 34. Harb, M.; Enquist, H.; Jurgilaitis, A.; Tuyakova, F. T.; Obraztsov, A. N.; Larsson, J. Phonon-Phonon Interactions in Photoexcited Graphite Studied by Ultrafast Electron Diffraction. *Phys. Rev. B* **2016**, *93*, 104104.
- 35. Wagman, D. D.; Kilpatrick, J. E.; Taylor, W. J.; Pitzer, K. S.; Rossini, F. D. Heats, Free Energies, and Equilibrium Constants of Some Reactions Involving O₂, H₂, H₂O, C, CO, CO₂, and CH₄. *J. Res. Nat. Bur. Stds.* **1945**, *34*, 143-161.
- 36. Butland, A. T. D.; Maddison, R. J. The Specific Heat of Graphite: An Evaluation of Measurements. *J. Nucl. Mater.* **1973**, *49*, 45-56.

- 37. Chebl, M.; He, X.; Yang, D.-S. Ultrafast Carrier-Coupled Interlayer Contraction, Coherent Intralayer Motions, and Phonon Thermalization Dynamics of Black Phosphorus. *Nano Lett.* **2022**, *22*, 5230-5235.
- 38. Krivchikov, A. I.; Sharapova, I. V.; Korolyuk, O. A.; Romantsova, O. O.; Bermejo, F. J. Experimental Evidence of the Role of Quasilocalized Phonons in the Thermal Conductivity of Simple Alcohols in Orientationally Ordered Crystalline Phases. *Low Temp. Phys.* **2009**, *35*, 891-897.
- 39. Stoner, R. J.; Maris, H. J. Kapitza Conductance and Heat Flow between Solids at Temperatures from 50 to 300 K. *Phys. Rev. B* **1993**, *48*, 16373-16387.
- 40. Talón, C.; Ramos, M. A.; Vieira, S.; Cuello, G. J.; Bermejo, F. J.; Criado, A.; Senent, M. L.; Bennington, S. M.; Fischer, H. E.; Schober, H. Low-Temperature Specific Heat and Glassy Dynamics of a Polymorphic Molecular Solid. *Phys. Rev. B* **1998**, *58*, 745-755.
- 41. Guzelturk, B.; Kamysbayev, V.; Wang, D.; Hu, H.; Li, R.; King, S. B.; Reid, A. H.; Lin, M.-F.; Wang, X.; Walko, D. A.; Zhang, X.; Lindenberg, A.; Talapin, D. V. Understanding and Controlling Photothermal Responses in MXenes. *Nano Lett.* **2023**, *23*, 2677-2686.
- 42. Krumhansl, J.; Brooks, H. The Lattice Vibration Specific Heat of Graphite. *J. Chem. Phys.* **1953**, *21*, 1663-1669.
- 43. Krivchikov, A. I.; Yushchenko, A. N.; Manzhelii, V. G.; Korolyuk, O. A.; Bermejo, F. J.; Fernández-Perea, R.; Cabrillo, C.; González, M. A. Scattering of Acoustic Phonons in Disordered Matter: A Quantitative Evaluation of the Effects of Positional Versus Orientational Disorder. *Phys. Rev. B* **2006**, *74*, 060201(R).
- 44. Korolyuk, O. A.; Krivchikov, A. I.; Sharapova, I. V.; Romantsova, O. O. Heat Transfer in Solid Methyl Alcohol. *Low Temp. Phys.* **2009**, *35*, 290-293.
- 45. Ungeheuer, A.; Hassanien, A. S.; Mir, M. T.; Nöding, L.; Baumert, T.; Senftleben, A. Selective Excitation of Higher Harmonic Coherent Acoustic Phonons in a Graphite Nanofilm. *J. Phys. Chem C* **2022**, *126*, 19822-19833.
- 46. Qi, R. S.; Shi, R. C.; Li, Y. H.; Sun, Y. W.; Wu, M.; Li, N.; Du, J. L.; Liu, K. H.; Chen, C. L.; Chen, J.; Wang, F.; Yu, D. P.; Wang, E.-G.; Gao, P. Measuring Phonon Dispersion at an Interface. *Nature* 2021, 599, 399-403.
- 47. Sääskilahti, K.; Oksanen, J.; Tulkki, J.; Volz, S. Spectral Mapping of Heat Transfer Mechanisms at Liquid-Solid Interfaces. *Phys. Rev. E* **2016**, *93*, 052141.